

Neural Network-Based IRS Assisted NLoS DoA Estimation

Yasin Azhdari and Mahmoud Farhang

Abstract—Direction-of-Arrival (DoA) estimation in challenging Non-Line-of-Sight (NLoS) environments is crucial for various wireless applications. This paper presents a novel neural network architecture to address this challenge using an Intelligent Reflecting Surface (IRS). The key innovation is the introduction of a dedicated, learnable Neural Network (NN)-based IRS layer integrated within a carefully designed network structure. Unlike conventional neural network layers, this specialized layer incorporates sinusoidal weight constraints, where the phase arguments of these sinusoids are learned during training to directly emulate the phase shifts of the IRS elements. This allows the network to autonomously optimize the IRS configuration for enhanced DoA estimation, eliminating the need for separate IRS control algorithms. We adapt standard backpropagation to accommodate these constraints, ensuring effective training. Numerical simulations, conducted under various conditions and noise levels, demonstrate the superior performance of the proposed approach compared to traditional methods, highlighting its potential for significantly improved DoA estimation accuracy in complex IRS-assisted wireless systems. Code for reproducing the results is available at: <https://github.com/yasinazhdari/Neural-Network-Based-IRS-Assisted-NLoS-DoA-Estimation>.

Index Terms—Direction of arrival (DoA) estimation, Intelligent Reflecting Surface (IRS), Neural Network (NN).

I. INTRODUCTION

ESTIMATION of parameters corresponding to exponential signals contaminated in noise is a crucial problem in various signal processing applications, including array signal processing [1]. Array signal processing aims to estimate parameters by exploiting both temporal and spatial information. Estimating the angular position of some sources by a set of sensors forming an array, known as Direction of Arrival (DoA) Estimation, is among main problems in the field of array signal processing. DoA estimation concerns determination of the angle of arrival of signals, in electromagnetic or acoustic wave forms, impinging on an array of antennas. DoA estimation has a variety of applications in wireless communications, sonar, radar, navigation and so on [2]–[7].

Intelligent Reflecting Surfaces (IRSs) or Reconfigurable Intelligent Surfaces (RISs) have been applied in numerous fields in recent years, including radars and wireless communications. The main characteristic of these surfaces is that they have adjustable phase, amplitude, frequency and polarization, i.e., tunable electromagnetic response [8]. Non-line of sight paths are established in dead zones by proper exploit of an IRS and adjustment of its reflection coefficients, where line of sight links do not exist [9].

An IRS-assisted approach is proposed to improve the SNR of received signals in order to enhance the performance of a detection system [10] by adjusting phases of the IRS.

Moreover, the phase of the IRS is adjusted to maximize the signal-to-noise ratio (SNR) in the direction corresponding to the user equipment for localization in wireless communication under near-field propagation regime [11]. In addition, the IRS-assisted scheme is employed for Direction of Arrival (DoA) estimation problem, too. For example, in [12], a coprime linear array (CLA) is implemented by controlling IRS units. Also a DoA estimation method is presented corresponding to the IRS-based CLA. In [13], a cost-effective direction-finding system using an unmanned aerial vehicle (UAV) swarm is presented. This system includes a central full-functional receiving unit that performs DoA estimation by solely receiving the signals reflected by the IRS. Furthermore, [14] explores a method where the array receiver collects both the reflected signal from the IRS and the direct-path signal. By designing the phase of the IRS, the reflected path can be leveraged to enhance the accuracy of DoA estimation. Additionally, [15] formulates and addresses the DoA estimation problem in the presence of wireless communication interference using an IRS. An atomic norm-based approach is then proposed for joint DoA estimation and interference removal, where the optimization problem is also solved to design the matrix containing IRS characteristics for interference mitigation.

An important subject under IRS-related topics is how to adjust and tune its response, specifically the phase response, in order to attain the desired performance. In related works phase design is implemented to maximize the SNR towards the desired user equipment, to maximize the coherence of the signals from direct and reflected paths, to minimize the Cramer-Rao Lower Bound (CRLB) of the problem, or to remove the interference [11], [14]–[16]. Though a reasonable way is to use Artificial Neural Networks (ANNs) to optimize the RIS phases, as far as we know, no particular task-based phase design using a dedicated Neural Network (NN) layer as the IRS layer itself has been proposed yet. This represents a significant gap in the literature that this paper addresses.

An Artificial Neural Network (ANN) has shown the capability to establish the mapping between some input features (usually the raw measurements or the correlation matrix) and directions of sources. Both fully-connected and convolutional neural networks with different modifications are used to address the problem of DoA estimation under variety of scenarios and have showed superior performance compared to the classical methods under certain conditions [17]–[22].

The main contribution of this paper is introduction of a novel layer for ANNs, which acts as the IRS (NN-based IRS layer) and providing its corresponding mathematics in order to learn the optimal phase design with respect to the

task of DoA estimation, which has not been done yet to our best knowledge. Also we will Compare the performance of the proposed learning-based method with the Maximum Likelihood (ML) estimate and also non learning methods modified for our specific problem model and formulation. In this research, Uniform Planar Arrays (UPAs) are considered. But the method can be extended to other types of arrays.

The remainder of this paper is structured as follows: The problem model and formulation is described in Section II. Section III reviews well-known non learning-based RIS assisted DoA estimation techniques and their corresponding algorithms. Section IV presents the novel NN-based RIS layer and its corresponding mathematics, employed in a well-thought-out neural network structures for the task of DoA estimation; numerical simulations and results are provided in Section V. Finally, conclusions are given in Section VI.

Notations: $j = \sqrt{-1}$ represents the imaginary unit. Boldface lower case letters refer to vectors and boldface upper case letters denote matrices. For a square matrix \mathbf{S} , \mathbf{S}^{-1} and $\text{tr}(\mathbf{S})$ denote its inverse and trace, respectively. For an arbitrary matrix \mathbf{M} , \mathbf{M}^T , \mathbf{M}^H , and \mathbf{M}^* are its transpose, conjugate transpose, and conjugate, respectively. The matrix \mathbf{I}_m represents the identity matrix with dimension $m \times m$. We use $CN(\mathbf{m}; \mathbf{C})$ to show the distribution of a complex Gaussian random vector with mean of vector \mathbf{m} and covariance of matrix \mathbf{C} . The real and imaginary parts of a complex number are denoted by $\text{Re}\{\cdot\}$ and $\text{Im}\{\cdot\}$, respectively. $|\cdot|$ represents the magnitude of a complex number and $\|\cdot\|$ stands for the Euclidean norm. $\text{diag}(a_1, \dots, a_N)$ represents the diagonalization operator which results in a diagonal matrix with diagonal elements of a_1, \dots, a_N . \odot denotes element-wise product between two matrices or vectors of the same dimension.

II. PROBLEM MODEL

A. Formulation

An IRS-assisted scenario as shown in Fig. 1 is considered. According to figure 1, it is assumed that there is no line of sight path between the source and the antenna array. Thus the only path available is through IRS reflection. The antenna array and the IRS are both considered to be uniform planar arrays (UPAs). The antenna array is placed on the yz plane of the coordinate system and the IRS is placed on the xy plane. The target is assumed to be in the far-field region with respect to the IRS and antennas, whereas the IRS is placed in the near-field region with respect to the antennas. Without loss of generality, one target at the non line of sight far-field region of the array is assumed, i.e., the most powerful one. Narrow-band waveform is assumed to prevent the effect of signal propagation on the IRS and the array. Also, unit gains and isotropic power receiving patterns are considered for both array antennas and IRS unit cells. As optimizing those factors are out of scope of this paper.

Let M_y^A and M_z^A denote the number of UPA elements along the y and z axes, with inter-element spacings of d_y^A and d_z^A , respectively. Similarly, let M_x^R and M_y^R denote the number of RIS unit cells along the x and y axes, with inter-element

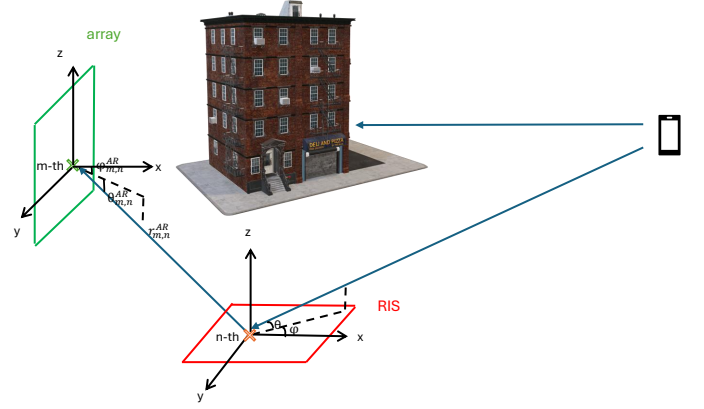


Fig. 1: Problem Model

spacings of d_x^R and d_y^R . $M^A = M_y^A \times M_z^A$ and $M^R = M_x^R \times M_y^R$ denote the total number of ULA elements and IRS unit cells, respectively. The angle between the wavefront incident on the IRS and its projection on the xy plane is denoted as θ . Moreover the angle between the projection on the xy plane and the x -axis is represented as ϕ . The position of the (m_y, m_z) -th UPA element is given as:

$$p_m^A = p_{m_y, m_z}^A = (0, m_y d_y^A, m_z d_z^A), \quad (1)$$

where $1 \leq m_y \leq M_y^A$, $1 \leq m_z \leq M_z^A$. The position of the (n_x, n_y) -th RIS unit cell is:

$$p_n^R = p_{n_x, n_y}^R = (n_x d_x^R, n_y d_y^R, 0), \quad (2)$$

where $1 \leq n_x \leq M_x^R$, $1 \leq n_y \leq M_y^R$.

The path difference for the signal from the source to the RIS and from the RIS to the UPA is now computed considering the spatial configuration. The distance between the (m_x, m_y) -th UPA element and the (n_x, n_y) -th RIS unit cell is:

$$r_{m,n}^{AR} = \|p_m^A - p_n^R\|_2. \quad (3)$$

Additionally, $\theta_{m,n}^{AR}$ denotes the angle between the n th IRS unit cell and the m th array element shown in Fig. 1, respectively. Moreover,

$$r_n^{RT} = r_{n_x, n_y}^{RT} = n_x \cos(\theta) \cos(\phi) + n_y \cos(\theta) \sin(\phi) \quad (4)$$

denotes the path difference between the reference phase cell and the n th IRS unit cell.

Also $\gamma_n = |\gamma_n| e^{j\phi_n}$ denote the adjustable reflection coefficient of the n th unit cell. $|\gamma_n|$ s are assumed to be 1 throughout this paper. Considering Φ as the IRS phase shifts vector, $\omega = e^{j\Phi} = [e^{j\phi_1}, e^{j\phi_2}, \dots, e^{j\phi_{M^R}}]$ denotes the corresponding reflective steering vector. Then Ω is defined as the $M^R \times M^R$ matrix containing the IRS phases as follows:

$$\Omega = \text{diag}(\omega) = \text{diag}([e^{j\phi_1}, e^{j\phi_2}, \dots, e^{j\phi_{M^R}}]) \quad (5)$$

Considering a far-field deterministic impinging source, the received signal from the reflection path can be modeled as [11], [14]:

$$\mathbf{y}_r = (\mathbf{H}^{AR} \odot \mathbf{A}^{AR}) \Omega \mathbf{a}^{RT} s = \mathbf{a}_r s \quad (6)$$

where \mathbf{A}^{AR} and \mathbf{a}^{RT} are the array-IRS steering matrix and IRS-target steering vector, respectively.

$$\mathbf{A}^{AR} = \begin{bmatrix} e^{-j2\pi r_{1,1}^{AR}/\lambda} \dots & e^{-j2\pi r_{1,M^R}^{AR}/\lambda} \\ \dots & \dots \\ e^{-j2\pi r_{M^A,1}^{AR}/\lambda} \dots & e^{-j2\pi r_{M^A,M^R}^{AR}/\lambda} \end{bmatrix} \quad (7)$$

$$\mathbf{a}^{RT} = [e^{j2\pi r_1^{RT}/\lambda}, \dots, e^{j2\pi r_{M^R}^{RT}/\lambda}]^T \quad (8)$$

Also, \mathbf{H}^{AR} is the matrix representing the amplitude of the received signal from the near-field reflection paths [23]

$$H_{m,n}^{AR} = \sqrt{\frac{\lambda^2}{(4\pi r_{m,n}^{AR})^2} P_r} \quad (9)$$

where P_r denotes the received power at the IRS.

Thus the received signal at array can be written as:

$$\mathbf{y} = \mathbf{y}_r + \mathbf{n} = (\mathbf{H}^{AR} \odot \mathbf{A}^{AR}) \Omega \mathbf{a}^{RT} s + \mathbf{n} = \mathbf{a}_r s + \mathbf{n} \quad (10)$$

where \mathbf{n} is the additive noise distributed as $CN(\mathbf{0}, \sigma_n^2 \mathbf{I})$.

The signal s in the above formulation can also represent a vector containing multiple snapshots of the source signal. In this case, s has dimensions $L \times 1$, where L is the number of snapshots. Consequently, the received signal \mathbf{y} becomes:

$$\mathbf{Y} = \mathbf{a}_r \mathbf{s} + \mathbf{N}, \quad (11)$$

where $\mathbf{Y} \in \mathbb{C}^{M^A \times L}$ is the matrix of received signals, $\mathbf{s} \in \mathbb{C}^{1 \times L}$ is the vector of source signals, and $\mathbf{N} \in \mathbb{C}^{M^A \times L}$ represents the noise matrix.

Furthermore, this model can be extended to account for multiple sources. Assuming K sources, the received signal becomes:

$$\mathbf{Y} = \sum_{k=1}^K \mathbf{a}_{r,k} \mathbf{s}_k + \mathbf{N}, \quad (12)$$

where $\mathbf{a}_{r,k}$ is the array response vector corresponding to the k th source, and $\mathbf{s}_k \in \mathbb{C}^{1 \times L}$ represents the snapshot signals of the k th source.

III. NON LEARNING-BASED RIS ASSISTED DOA ESTIMATION

A. Phase adjustment method

Considering the fact that in the aforementioned non line of sight scenario, maximizing the coherence between direct and reflected path signals can not be considered, and also due to the fact that the phase adjustment based on maximizing the received SNR at the array antenna is outperformed by CRLB minimization criterion [16], minimizing the CRLB by selecting proper set of phases Φ in our specific problem model is considered [14].

$$\min_{\omega} (\text{CRLB}_{\theta}(\omega) + \text{CRLB}_{\phi}(\omega)) \quad \text{s.t.} \quad |\omega_i| = 1 \quad \forall i = 1, \dots, M^R \quad (13)$$

where $\text{CRLB}_{\theta}(\omega)$ and $\text{CRLB}_{\phi}(\omega)$ for our specific problem model and formulation, can be obtained in a similar fashion to [24] (signal and noise variance are assumed to be known):

$$\text{CRLB}_{\theta} = \frac{\sigma_n^2}{2\sigma_s^2} \text{Re} \left\{ \frac{\partial \mathbf{a}_r}{\partial \theta}^H (I - \mathbf{a}_r (\mathbf{a}_r^H \mathbf{a}_r)^{-1} \mathbf{a}_r^H) \frac{\partial \mathbf{a}_r}{\partial \theta} \right\}^{-1} \quad (14)$$

and

$$\text{CRLB}_{\phi} = \frac{\sigma_n^2}{2\sigma_s^2} \text{Re} \left\{ \frac{\partial \mathbf{a}_r}{\partial \phi}^H (I - \mathbf{a}_r (\mathbf{a}_r^H \mathbf{a}_r)^{-1} \mathbf{a}_r^H) \frac{\partial \mathbf{a}_r}{\partial \phi} \right\}^{-1} \quad (15)$$

where $\sigma_s^2 = E\{\|s\|^2\} = \|s\|^2$. Because the CRLB function and the unit-modulus constraints are not convex, The optimization problem of the IRS phase design is not convex and thus is challenging and complicated. In order to transform this problem into a convex optimization problem, the semi definite relaxation (SDR) and successive convex approximation (SCA) techniques can be employed [16]. Also the method of Riemannian manifold optimization can be applied for designing optimal phase shifts [14]. Here we have complex circle manifold, and to solve the Riemannian manifold-based optimization problem (13) the Riemannian Steepest Descent (SD), Conjugate Gradient (CG), and Trust-Region (TR) methods are proposed before [25]. Here the CG method is considered.

B. Doa estimation methods

1) *Maximum Likelihood Doa Estimation*: The Maximum Likelihood (ML) DoA estimator for a deterministic source signal is implemented as follows and requires a grid search [26]:

$$\hat{\theta}, \hat{\phi} = \underset{\theta, \phi}{\text{argmax}} \lambda_{\max} [(\mathbf{a}_r^H \mathbf{a}_r)^{-\frac{1}{2}} (\mathbf{a}_r^H \mathbf{y} \mathbf{y}^H \mathbf{a}_r) (\mathbf{a}_r^H \mathbf{a}_r)^{-\frac{1}{2}}] \quad (16)$$

where $\lambda_{\max}[\mathbf{M}]$ represents the maximum eigenvalue of the matrix \mathbf{M} .

2) *MUSIC*: The MUSIC (Multiple Signal Classification) algorithm [27] is a widely-used subspace-based direction-of-arrival (DoA) estimation technique. It operates by separating the orthogonal noise and signal subspaces, which are derived from the eigenvectors of the covariance matrix ($\mathbf{R} = E\{\mathbf{y} \mathbf{y}^H\}$). Specifically, if \mathbf{v}_1 to \mathbf{v}_M are the eigenvectors of \mathbf{R} , sorted in descending order of their corresponding eigenvalues, and K is the number of sources, the MUSIC output power is then defined as:

$$P(\theta, \phi) = \frac{1}{\sum_{i=K+1}^M |\mathbf{a}_r^H \mathbf{v}_i|^2} = \frac{1}{\mathbf{a}_r^H \mathbf{V}_n \mathbf{V}_n^H \mathbf{a}_r} \quad (17)$$

where \mathbf{v}_{K+1} to \mathbf{v}_M form the matrix \mathbf{V}_n .

3) *Compressed Sensing (CS)-based Doa Estimation*: The sparse reconstruction problem for the multiple measurement vector case is expressed as follows [28]:

$$\min_{\mathbf{X}} \frac{1}{2} \|\mathbf{Y} - \mathbf{A}_{\text{dict.}} \mathbf{X}\|_{2,2}^2 + \tau \|\mathbf{X}\|_{2,1} \quad (18)$$

where the over completed dictionary $\mathbf{A}_{\text{dict.}}$ of size $M^A \times M^D$ is given as $\mathbf{A}_{\text{dict.}} = [\mathbf{a}(\theta_1), \mathbf{a}(\theta_2), \dots, \mathbf{a}(\theta_{M^D})]$, the sparse spatial spectrum is denoted as \mathbf{X} , and the non negative regularization parameter is represented as τ which can be determined by [28]:

$$\tau = \sqrt{\frac{M^D L \sigma_n^2}{K}} \quad (19)$$

where L , K denote the number of snapshots and the number of sources, respectively. The convex problem (18) can be tackled by interior-point algorithm-based packages, i.e., CVX [29].

IV. LEARNING-BASED IRS ASSISTED DOA ESTIMATION

As previously discussed, various non-learning-based optimization methods have been proposed to adjust the phases of IRS units. In this paper, we propose a novel approach by implementing the IRS using a dedicated neural network layer. This layer is designed to learn phase adjustments specifically tailored for the task of Direction of Arrival (DoA) estimation. The corresponding mathematical formulation and the overall network structure are also presented.

The network processes raw measurements observed at the IRS as its inputs. Since the inputs to a neural network must be real-valued, the complex measurements obtained at each IRS unit are pre-processed by separating their real and imaginary components. The pre-processed measurements are subsequently passed to the IRS layer.

Unlike standard neural network layers with tunable constant weights, the IRS layer requires weights that are sinusoidal in nature, where the arguments (or phases) of these weights must be optimized during the training process. Consequently, both the forward propagation (FP) and backward propagation (BP) procedures must be adapted to accommodate this unique weight structure.

The IRS layer applies a linear activation function. The following subsections detail the implementation of this process.

A. Feed Forward and Backward Propagation

Neural networks operate through two fundamental processes: forward propagation (FP) and backward propagation (BP). These processes form the backbone of training and optimization. Consider a fully connected (FC) layer characterized by an input vector $\mathbf{x} \in \mathbb{R}^{M \times 1}$, a weight matrix $\mathbf{W} \in \mathbb{R}^{N \times M}$, a bias vector $\mathbf{b} \in \mathbb{R}^{N \times 1}$, and an output vector $\mathbf{y} \in \mathbb{R}^{N \times 1}$. Forward propagation for this layer is mathematically expressed as:

$$\text{FP: } \mathbf{y} = \mathbf{W}\mathbf{x} + \mathbf{b}. \quad (20)$$

The resulting output serves as the input to the subsequent layer. Based on the final predicted output and the target values,

an error term E is calculated and back propagated in the network. The goal of training is to minimize this error by updating the layer's parameters through backward propagation (BP), typically using gradient descent.

In BP, the gradients of the error with respect to the layer's parameters, $\frac{\partial E}{\partial \mathbf{W}}$ and $\frac{\partial E}{\partial \mathbf{b}}$, as well as with respect to the input, $\frac{\partial E}{\partial \mathbf{x}}$, are computed using the chain rule. Assuming that the derivative of the error with respect to the output, $\frac{\partial E}{\partial \mathbf{y}}$, is known, these gradients are calculated as:

$$\frac{\partial E}{\partial \mathbf{W}} = \frac{\partial E}{\partial \mathbf{y}} \mathbf{x}^T, \quad (21)$$

$$\frac{\partial E}{\partial \mathbf{b}} = \frac{\partial E}{\partial \mathbf{y}}, \quad (22)$$

$$\frac{\partial E}{\partial \mathbf{x}} = \mathbf{W}^T \frac{\partial E}{\partial \mathbf{y}}. \quad (23)$$

B. Proposed IRS Layer Mechanism

1) *Mathematical Foundation*: Consider a complex-valued element of the observation vector of the IRS: $z_i = a_i + jb_i$ for $i = 1, \dots, M^R$, where a_i and b_i denote the real and imaginary components, respectively. Multiplying this observation by a complex exponential $e^{j\omega_i}$ results in the following expression:

$$z_i e^{j\omega_i} = (a_i + jb_i)(\cos(\omega_i) + j \sin(\omega_i)). \quad (24)$$

where the product yields in the following final result per each element:

$$z_i e^{j\omega_i} = (a_i \cos(\omega_i) - b_i \sin(\omega_i)) + j(a_i \sin(\omega_i) + b_i \cos(\omega_i)). \quad (25)$$

Separating the real and imaginary components of the result and interleaving them for each element, this operation can be expressed in the matrix form. By interleaving the real and imaginary parts of the observations into a single vector as follows:

$$\mathbf{z} = [a_1, b_1, a_2, b_2, \dots, a_{M^R}, b_{M^R}]^T. \quad (26)$$

The transformation is then achieved through a block diagonal matrix \mathbf{W} , where each 2×2 block \mathbf{W}_i is parameterized by the phase angle ω_i :

$$\mathbf{W}_i = \begin{bmatrix} \cos(\omega_i) & \sin(\omega_i) \\ -\sin(\omega_i) & \cos(\omega_i) \end{bmatrix}. \quad (27)$$

The complete block diagonal weight matrix \mathbf{W} is then represented as:

$$\mathbf{W} = \text{diag}(\mathbf{W}_1, \mathbf{W}_2, \dots, \mathbf{W}_{M^R}). \quad (28)$$

Finally, the transformed vector \mathbf{z}' , which includes the interleaved real and imaginary parts of the desired result, is obtained as:

$$\mathbf{z}' = \mathbf{W}\mathbf{z}. \quad (29)$$

This formulation reveals that the multiplication of each complex observation $z_i = a_i + jb_i$ by $e^{j\omega_i}$ for $i = 1, \dots, M^R$ can be equivalently performed by applying a block diagonal transformation matrix \mathbf{W} to the interleaved real and imaginary parts.

2) *Definition of the Weight Matrix*: The proposed IRS layer employs the weight matrix \mathbf{W} , consisting of M^R trainable 2×2 blocks, described in the previous part. Each block is parameterized by a single variable ω_i , corresponding to a phase adjustment:

$$\mathbf{W}_i = \begin{bmatrix} \cos(\omega_i) & \sin(\omega_i) \\ -\sin(\omega_i) & \cos(\omega_i) \end{bmatrix}, \quad i = 1, \dots, M^R. \quad (30)$$

The parameters ω_i are initialized uniformly within $[-\pi, \pi]$ and updated during training to optimize the phase adjustments for the observations.

3) *Forward Propagation with the IRS Layer*: In the forward pass, the IRS layer applies the block diagonal transformation \mathbf{W} to the input vector \mathbf{x} , which consists of the interleaved real and imaginary components of the IRS observations. The output of the layer, which has the same dimension as input, is formulated as follows (no biases are considered for this layer):

$$\mathbf{y} = \mathbf{W}\mathbf{x}. \quad (31)$$

4) *Backward Propagation for the IRS Layer*: The backward pass involves calculating the gradients of the loss function E with respect to the trainable parameters ω_i and the inputs \mathbf{x} .

Each block \mathbf{W}_i is parameterized by ω_i , and the derivative of \mathbf{W}_i with respect to ω_i is:

$$\frac{\partial \mathbf{W}_i}{\partial \omega_i} = \begin{bmatrix} -\sin(\omega_i) & \cos(\omega_i) \\ -\cos(\omega_i) & -\sin(\omega_i) \end{bmatrix}. \quad (32)$$

Since $\mathbf{y} = \mathbf{W}\mathbf{x}$, and \mathbf{W} is block diagonal, only the elements y_{2i-1} and y_{2i} depend on ω_i . Therefore:

$$\begin{aligned} \frac{\partial y_{2i-1}}{\partial \omega_i} &= \begin{bmatrix} 1 & 0 \end{bmatrix} \frac{\partial \mathbf{W}_i}{\partial \omega_i} \begin{bmatrix} x_{2i-1} \\ x_{2i} \end{bmatrix} \\ &= -x_{2i-1} \sin(\omega_i) + x_{2i} \cos(\omega_i) \end{aligned} \quad (33)$$

$$\begin{aligned} \frac{\partial y_{2i}}{\partial \omega_i} &= \begin{bmatrix} 0 & 1 \end{bmatrix} \frac{\partial \mathbf{W}_i}{\partial \omega_i} \begin{bmatrix} x_{2i-1} \\ x_{2i} \end{bmatrix} \\ &= -x_{2i-1} \cos(\omega_i) - x_{2i} \sin(\omega_i) \end{aligned} \quad (34)$$

Using the chain rule, the gradient of the loss with respect to ω_i is:

$$\frac{\partial E}{\partial \omega_i} = \frac{\partial E}{\partial y_{2i-1}} \frac{\partial y_{2i-1}}{\partial \omega_i} + \frac{\partial E}{\partial y_{2i}} \frac{\partial y_{2i}}{\partial \omega_i}. \quad (35)$$

Moreover, the gradient of the loss with respect to the inputs \mathbf{x} is computed as:

$$\frac{\partial E}{\partial \mathbf{x}} = \left(\frac{\partial E}{\partial \mathbf{y}} \right)^T \mathbf{W}. \quad (36)$$

The trainable parameters ω_i are then updated using gradient descent:

$$\omega_i \leftarrow \omega_i - \eta \cdot \frac{\partial E}{\partial \omega_i}, \quad (37)$$

where η is the learning rate. This procedure ensures convergence to optimal phase adjustments during the training.

The Mean Squared Error (MSE) is employed as the loss function for the DoA regression task:

$$E = \frac{1}{n} \sum_{i=1}^n (y_i^* - y_i)^2, \quad (38)$$

where y_i^* and y_i are the ground truth and predicted outputs, respectively. Besides, the gradient of the loss with respect to \mathbf{y} is:

$$\frac{\partial E}{\partial \mathbf{y}} = \frac{2}{n} (\mathbf{y} - \mathbf{y}^*). \quad (39)$$

5) *Key Advantages of the Proposed IRS Layer*:

- **Novelty**: Unlike conventional layers, the proposed IRS layer explicitly models the phase-shifting behavior of IRS-aided systems using a trainable block diagonal matrix. This is a unique contribution to the field.
- **Efficiency**: By parameterizing each 2×2 block with a single phase variable ω_i , the IRS layer achieves a compact representation with minimal computational overhead.
- **Differentiability**: The sinusoidal structure of the weight matrix ensures smooth gradients, facilitating effective training using backpropagation.
- **Relevance**: The layer directly aligns with the physical principles of IRS-aided communication, bridging the gap between theoretical models and practical implementation.

These features underscore the innovation and applicability of the proposed IRS layer in modern deep learning architectures for DoA estimation and also other parameter estimation tasks.

C. Implementation of the network

The inputs of the network are the observations of the IRS unit cells. Thus in order to formulate the input of the network we consider the target-IRS link as a direct path and formulate IRS observations as the following:

$$\mathbf{x} = \mathbf{a}^{RT} \mathbf{s} + \mathbf{n} \quad (40)$$

where \mathbf{x} denotes the observations of IRS unit cells. Also, \mathbf{a}^{RT} and \mathbf{n} represent the IRS-target steering vector and the additive noise as discussed before.

In the pre-processing phase, the real and imaginary components of observation of each unit are extracted. A new observation vector is then constructed by interleaving the imaginary components with their respective real counterparts. Subsequent to this, a normalization is applied to bound the measurements between -1 and +1.

Next, the measurements are summarized up in one snapshot using a convolutional and recurrent based structure to summarize both spatial and temporal information prior to feeding them to the IRS layer.

Following IRS layer, a fixed layer is employed to implement the mapping of IRS observations to array measurements using the fixed weight matrix as defined in equation (6). This mapping is determined based on the geometric configuration of the problem, which remains constant throughout.

Subsequently, a DoA regressor is applied. The complete network architecture is illustrated in Fig. 2.

Scheme of the overall network with corresponding details is illustrated in Fig. 3 with simulation settings described in the next section. The output size of the Gated Recurrent Unit (GRU) [30] equals the number of input features per each snapshot. The number of nodes corresponding to the output layer is determined based on the number of sources (for

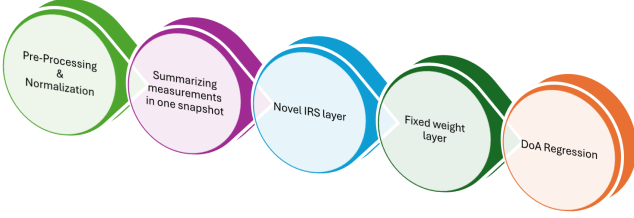


Fig. 2: The overall network structure

example is equal to 2 for the case of one source, representing elevation and azimuth angles). Due to the fact that input measurements contain both positive and negative values with the same probability, activation functions are chosen to be linear and $\tanh(\cdot)$ through the network.

Finally, a supervised DoA regression network is implemented. Thus the overall network can be represented with the following transform

$$\hat{\theta} = \mathbf{N}(\mathbf{x}) = \text{DoANET}(\mathbf{W} \cdot \mathbf{R}(\mathbf{S}(\mathbf{P}(\mathbf{x})))) \quad (41)$$

where $\mathbf{P}(\cdot)$ represents the pre-processing and normalization performed, $\mathbf{S}(\cdot)$ represents the summarizing stage based on conv1D and GRU units, $\mathbf{R}(\cdot)$ represents the novel IRS layer, and \mathbf{W} represents the fixed weight matrix. Finally, $\text{DoANET}(\cdot)$ represents the network associated with the DoA regression.

The overall network, including both the IRS block and the DoA estimator block will be tuned and adjusted simultaneously during the training phase concerning the ultimate task of DoA estimation. The details and parameters of the network and also the generation procedure of the corresponding datasets are presented in the next section, where the performance of the proposed scheme is compared with other IRS-based DoA estimation methods through simulations.

V. NUMERICAL SIMULATIONS AND RESULTS

A. Setup

The number of array elements and the number of IRS unit cells are assumed to be the same and equal to 5 at each dimension (25 in total). The problem model with simulation presets is illustrated in Fig. 4. The source signal is assumed to be a narrow-band deterministic exponential with a frequency of 1 GHz. Since the far-field range includes distances greater than $\frac{2D^2}{\lambda}$ (where D denotes the largest antenna dimension) and respecting that for the IRS and the array, the inter-element spacing is considered to be $\lambda/4$ and $\lambda/2$, respectively, $D = (M^R - 1)\lambda/2 = (M^A - 1)\lambda/2 = 2.5\lambda = 0.75\text{m}$. Thus, the far-field range in our considered setup will be any

distance greater than 3.75 meters. Based on the above far-field range threshold, we have considered the distances mentioned in Fig. 4.

The optimization process for training the neural network employs the Adam optimizer. The initial learning rate is set to 0.015, providing a balanced starting point that allows the model to converge efficiently. Training is conducted with a batch size of 64, ensuring that each update step is based on a representative sample of the data, which helps in stabilizing the learning process. The model is trained over 100 epochs, providing ample opportunity for the network to learn the underlying patterns in the data. To further enhance the training process and prevent overfitting, we implement early stopping and learning rate reduction callbacks. Moreover, as described before, the loss function is assumed to be the RMSE.

Initialization for both manifold-based optimization algorithm phases and also the sinusoidal weights phases of the RIS layer is done based on a uniform distribution over the set $[-\pi, \pi]$.

B. DataSets

For training, we generate a dataset of $N_{train} = 10,000$ examples for each source, where each example is an input-DoA pair $(\mathbf{x}, (\theta, \phi))$. We consider scenarios with one and four sources, beginning with a single snapshot. The source direction-of-arrival angles, elevation (θ) and azimuth (ϕ), are uniformly distributed within the FoV of 0° to 90° and 0° to 180° , respectively, with a resolution of 0.5° . The signal-to-noise ratio (SNR) values are selected independently from the set $\{-10, -5, 0, 5, 10\}$ dB using a uniform distribution.

The test set consists of $N_{test} = 100$ examples for each SNR value. The reported performance is the average over these independent test realizations.

Non-learning methods utilize the same simulation settings.

C. Experiments

Our initial investigation focuses on evaluating the contribution of the IRS layer to the system performance. The root mean squared error (RMSE) is used as the performance metric and is plotted against the signal-to-noise ratio (SNR) for both elevation and azimuth angles in Fig. 5. The RMSE for elevation angle is defined as:

$$\text{RMSE} = \sqrt{\frac{1}{C} \sum_{c=1}^C (\hat{\theta}_c - \theta)^2}, \quad (42)$$

where C represents the number of Monte Carlo simulations (set to 100), θ denotes the actual angular location of the source, and $\hat{\theta}_c$ represents the estimated angular location obtained in the c -th simulation run (expressed in degrees). Similarly, the RMSE for azimuth angle is defined.

To observe the effectiveness of the learning-based IRS layer, we compare a system employing the trainable IRS layer with a baseline system where the IRS phases are fixed randomly throughout training. Under a single-source assumption and utilizing a single snapshot (the summarizing network architecture, comprising 1D convolutional and GRU

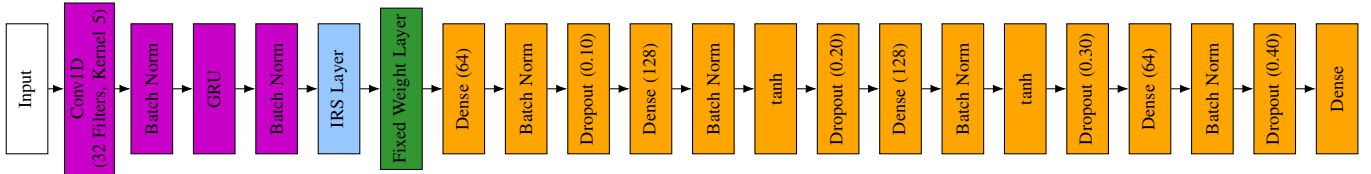


Fig. 3: Architecture of the Neural Network.

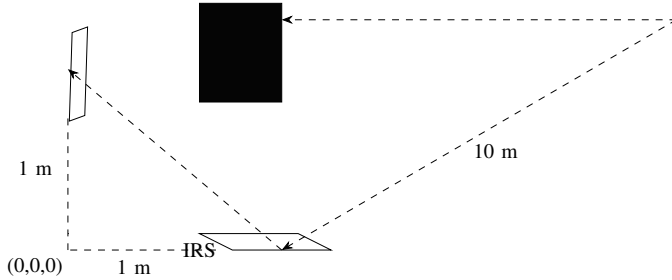


Fig. 4: Problem Model with Simulation Presets

layers, is bypassed for this evaluation), we demonstrate the performance gains attributable to trainable IRS layer. As illustrated in Fig. 5, optimizing the IRS phases during training (denoted by optimized phases) yields superior direction-of-arrival estimation performance compared to the random phase configuration (denoted by random fixed phases). This performance enhancement is observed for both elevation and azimuth angle estimation, highlighting the significant advantage of the trainable IRS layer.

Next, we conduct a comparative performance analysis of the proposed learning-based method and several classical direction-of-arrival (DoA) estimation techniques: Maximum Likelihood (ML), MUSIC, and Compressed Sensing (CS). This evaluation is performed assuming 10 snapshots and a randomly located source within the field of view (FoV), with the results depicted in Fig. 6. The resulting RMSE is averaged on 100 independent Monte Carlo runs.

The results demonstrate that the proposed neural network-based IRS-assisted DoA estimator achieves superior performance compared to the non-learning-based methods across the entire range of considered SNR values.

Moreover, a key advantage of the learning-based approach is its computational efficiency. Unlike the classical methods, which necessitate performing manifold optimization for every test instance, the neural network provides rapid estimations after training.

In the next experiment, we evaluate the performance of the proposed learning-based method and other non-learning-based methods (ML, MUSIC, and CS) under a two-source scenario, with the sources randomly distributed within the FoV. The results, shown in Fig. 7, confirm that the learning-based approach maintains its performance advantage under this more challenging scenario.

The final experiment assesses the impact of varying the number of snapshots on DOA estimation accuracy. This is a critical evaluation, as practical scenarios often involve limited data samples. We considered an SNR of 0 dB and a randomly

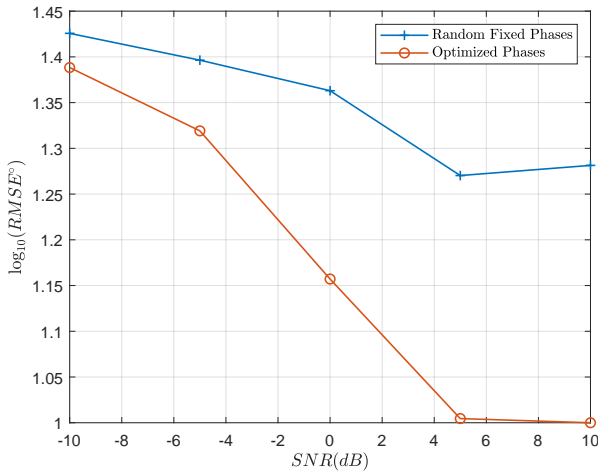
located source, varying the number of snapshots from 2 to 10. For each snapshot count, the RMSE was averaged over 100 independent Monte Carlo trials. Importantly, the neural network was trained using data with 10 snapshots and subsequently tested on data with fewer snapshots without retraining. This tests the network’s ability to generalize to unseen data conditions. The results, presented in Fig. 8, demonstrate that the learning-based methods maintain competitive or superior performance compared to classical methods, even when the number of available snapshots is significantly reduced. This highlights the potential of the proposed approach for real-world applications with limited data.

VI. CONCLUSION

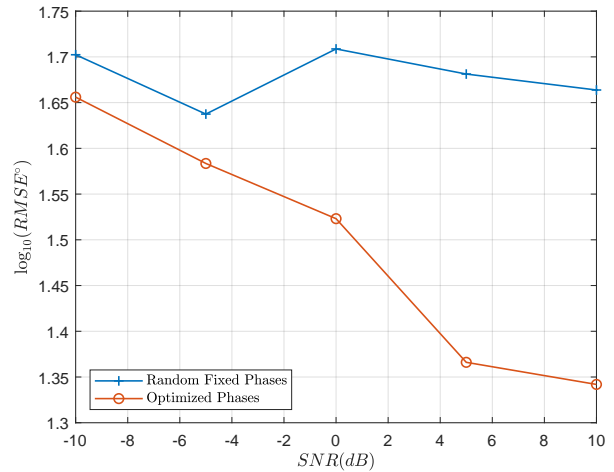
This paper proposes a novel neural network-based solution for IRS-assisted DoA estimation, centered around a new NN-based IRS layer. The neural network architecture is carefully designed to incorporate the necessary considerations in modeling the problem, enabling the network to effectively learn and adjust the IRS phase configurations. This integrated approach unifies the processes of IRS phase adjustment and DoA estimation, eliminating the need for separate, often complex, optimization algorithms. Numerical simulations across various scenarios confirm the effectiveness and robustness of the proposed method, demonstrating superior performance compared to existing non-learning-based DoA estimation techniques in IRS-assisted NLoS environments.

REFERENCES

- [1] H. Ye and D. DeGroat, “Maximum likelihood doa estimation and asymptotic cramer-rao bounds for additive unknown colored noise,” *IEEE Transactions on Signal Processing*, vol. 43, no. 4, pp. 938–949, 1995.
- [2] H. Krim and M. Viberg, “Two decades of array signal processing research: the parametric approach,” *IEEE signal processing magazine*, vol. 13, no. 4, pp. 67–94, 1996.
- [3] H. L. Van Trees, *Optimum array processing: Part IV of detection, estimation, and modulation theory*. Wiley-Interscience, 2008.
- [4] P.-J. Chung, M. Viberg, and J. Yu, “Doa estimation methods and algorithms,” in *Academic Press Library in Signal Processing*. Elsevier, 2014, vol. 3, pp. 599–650.
- [5] R. O. Nielsen, *Sonar signal processing*. Artech House, Inc., 1991.
- [6] Z. Chen, G. Gokeda, and Y. Yu, *Introduction to Direction-of-arrival Estimation*. Artech House, 2010.
- [7] T. E. Tuncer and B. Friedlander, *Classical and modern direction-of-arrival estimation*. Academic Press, 2009.
- [8] C. Huang, A. Zappone, G. C. Alexandropoulos, M. Debbah, and C. Yuen, “Reconfigurable intelligent surfaces for energy efficiency in wireless communication,” *IEEE transactions on wireless communications*, vol. 18, no. 8, pp. 4157–4170, 2019.
- [9] D. Dardari, N. Decarli, A. Guerra, and F. Guidi, “Los/nlos near-field localization with a large reconfigurable intelligent surface,” *IEEE Transactions on Wireless Communications*, vol. 21, no. 6, pp. 4282–4294, 2021.

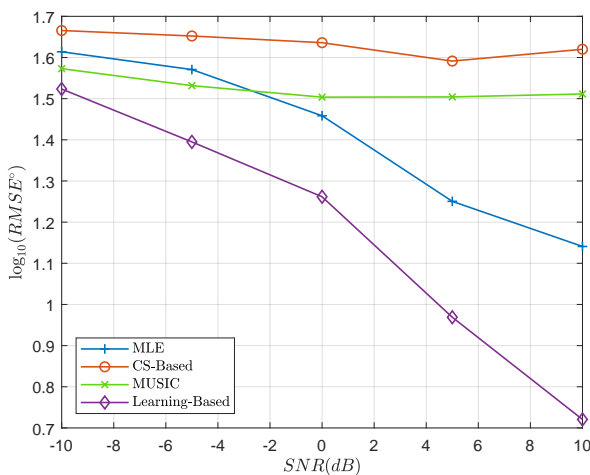


(a) Elevation Angle

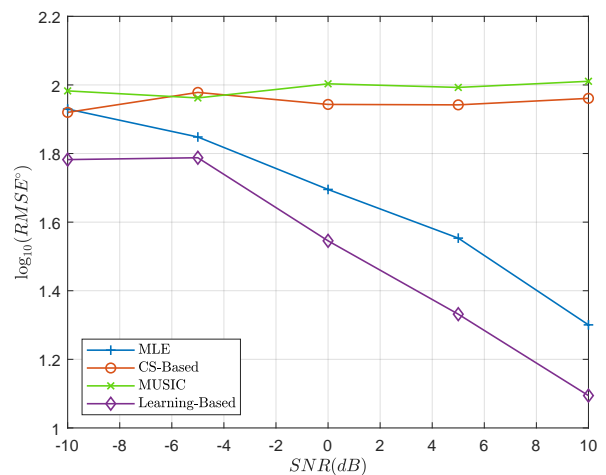


(b) Azimuth Angle

Fig. 5: Optimized Phases vs. Random Fixed Phases



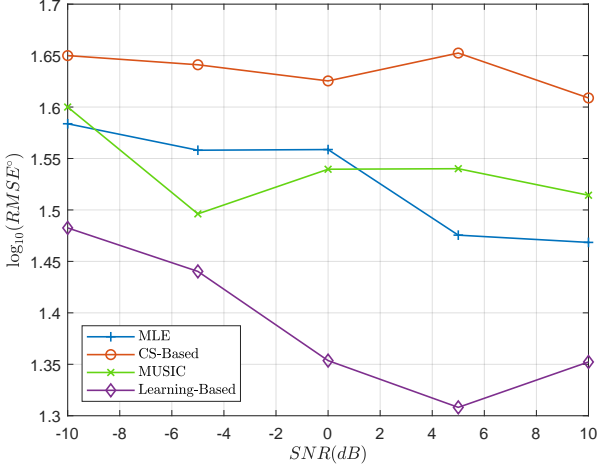
(a) Elevation Angle



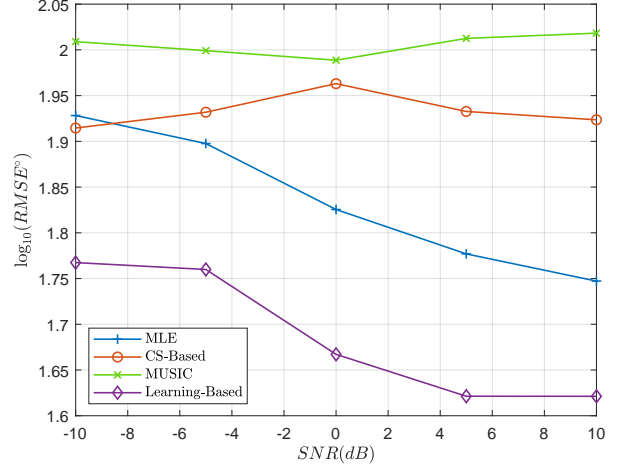
(b) Azimuth Angle

Fig. 6: RMSE vs. SNR - Learning vs. Non-learning - One Randomly Positioned Source

- [10] S. Buzzi, E. Grossi, M. Lops, and L. Venturino, "Radar target detection aided by reconfigurable intelligent surfaces," *IEEE Signal Processing Letters*, vol. 28, pp. 1315–1319, 2021.
- [11] A. Elzanaty, A. Guerra, F. Guidi, and M.-S. Alouini, "Reconfigurable intelligent surfaces for localization: Position and orientation error bounds," *IEEE Transactions on Signal Processing*, vol. 69, pp. 5386–5402, 2021.
- [12] T. Lan, K. Huang, L. Jin, X. Xu, X. Sun, and Z. Zhong, "Doa estimation algorithm for reconfigurable intelligent surface co-prime linear array based on multiple signal classification approach," *Information*, vol. 13, no. 2, p. 72, 2022.
- [13] P. Chen, Z. Chen, B. Zheng, and X. Wang, "Efficient doa estimation method for reconfigurable intelligent surfaces aided uav swarm," *IEEE Transactions on Signal Processing*, vol. 70, pp. 743–755, 2022.
- [14] H. Chen, Y. Bai, Q. Wang, H. Chen, L. Tang, and P. Han, "Doa estimation assisted by reconfigurable intelligent surfaces," *IEEE Sensors Journal*, 2023.
- [15] Z. Chen, P. Chen, Z. Guo, Y. Zhang, and X. Wang, "A ris-based vehicle doa estimation method with integrated sensing and communication system," *IEEE Transactions on Intelligent Transportation Systems*, 2023.
- [16] X. Song, J. Xu, F. Liu, T. X. Han, and Y. C. Eldar, "Intelligent reflecting surface enabled sensing: Cramér-rao bound optimization," *IEEE Transactions on Signal Processing*, 2023.
- [17] M. Agatonović, Z. Stanković, N. Dončov, L. Sit, B. Milovanović, and T. Zwick, "Application of artificial neural networks for efficient high-resolution 2d doa estimation," *Radioengineering*, vol. 21, no. 4, pp. 1178–1186, 2012.
- [18] J. Fuchs, R. Weigel, and M. Gardill, "Single-snapshot direction-of-arrival estimation of multiple targets using a multi-layer perceptron," in *2019 IEEE MTT-S International Conference on Microwaves for Intelligent Mobility (ICMIM)*. IEEE, 2019, pp. 1–4.
- [19] Y. Liu, H. Chen, and B. Wang, "Doa estimation based on cnn for underwater acoustic array," *Applied Acoustics*, vol. 172, p. 107594, 2021.
- [20] S. Feintuch, J. Tabrikian, I. Bilik, and H. Permuter, "Neural-network-based doa estimation in the presence of non-gaussian interference," *IEEE Transactions on Aerospace and Electronic Systems*, vol. 60, no. 1, pp. 119–132, 2023.
- [21] K. Liu, X. Wang, J. Yu, and J. Ma, "Attention based doa estimation in the presence of unknown nonuniform noise," *Applied Acoustics*, vol. 211, p. 109506, 2023.
- [22] S. Zheng, Z. Yang, W. Shen, L. Zhang, J. Zhu, Z. Zhao, and X. Yang, "Deep learning-based doa estimation," *IEEE Transactions on Cognitive Communications and Networking*, 2024.

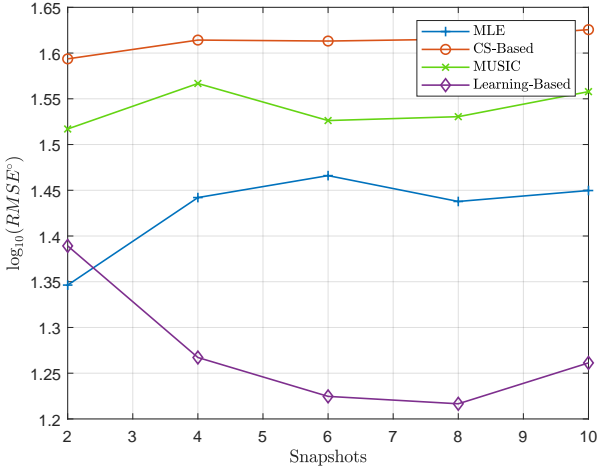


(a) Elevation Angles

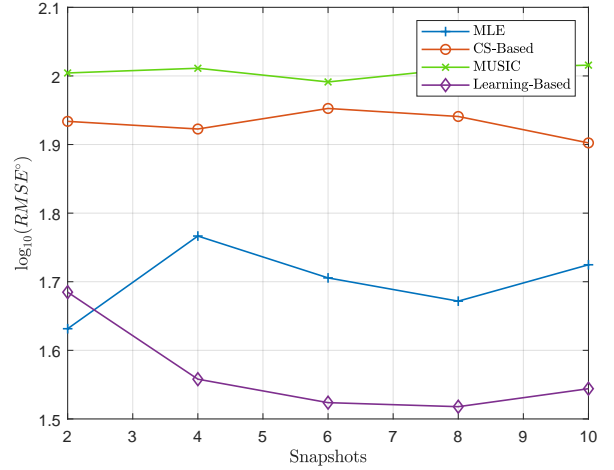


(b) Azimuth Angles

Fig. 7: RMSE vs. SNR - Learning vs. Non-learning - Two Randomly Positioned Sources



(a) Elevation Angle



(b) Azimuth Angle

Fig. 8: RMSE vs. Number of Snapshots - Learning vs. Non-learning

- [23] W. Tang, M. Z. Chen, X. Chen, J. Y. Dai, Y. Han, M. Di Renzo, Y. Zeng, S. Jin, Q. Cheng, and T. J. Cui, "Wireless communications with reconfigurable intelligent surface: Path loss modeling and experimental measurement," *IEEE transactions on wireless communications*, vol. 20, no. 1, pp. 421–439, 2020.
- [24] P. Stoica and A. Nehorai, "Music, maximum likelihood, and cramer-rao bound," *IEEE Transactions on Acoustics, speech, and signal processing*, vol. 37, no. 5, pp. 720–741, 1989.
- [25] N. Boumal, *An introduction to optimization on smooth manifolds*. Cambridge University Press, 2023. [Online]. Available: <https://www.nicolasboumal.net/book>
- [26] K. Boman and P. Stoica, "Low angle estimation: models, methods, and bounds," *Digital Signal Processing*, vol. 11, no. 1, pp. 35–79, 2001.
- [27] R. Schmidt, "Multiple emitter location and signal parameter estimation," *IEEE transactions on antennas and propagation*, vol. 34, no. 3, pp. 276–280, 1986.
- [28] H. Chen, Y. Wei, Y. Bai, and X. Zhang, "Sparse recovery for doa estimation with a reflection path," *IEEE Access*, vol. 6, pp. 70572–70581, 2018.
- [29] M. Grant and S. Boyd, "Cvx: Matlab software for disciplined convex programming, version 2.1," 2014.
- [30] K. Cho, B. Van Merriënboer, C. Gulcehre, D. Bahdanau, F. Bougares, H. Schwenk, and Y. Bengio, "Learning phrase representations using rnn encoder-decoder for statistical machine translation," *arXiv preprint arXiv:1406.1078*, 2014.